AGU ADVANCING EARTH AND SPACE SCIENCES

Geophysical Research Letters

RESEARCH LETTER
10.1029/2025GL117784

ColdBlobMIP: A Multi-Model Assessment of the Atmospheric Response to the North Atlantic Warming Hole

Sydney M. Kramer[1,2,3], Kristopher B. Karnauskas[1,2], Maxwell T. Elling[1,2], Lei Zhang[4], Heng Liu[4], Yanying Chen[4], Dillon J. Amaya[5], Larissa Nazarenko[6,7], Wenchang Yang[8], Gabriel A. Vecchi[8,9], Dervla Meegan-Kumar[10], Jane W. Baldwin[10], and Dhrubajyoti Samanta[11]

[1]Department of Atmospheric and Oceanic Sciences, University of Colorado Boulder, Boulder, CO, USA, [2]Cooperative Institute for Research in Environmental Sciences, University of Colorado Boulder, Boulder, CO, USA, [3]Lamont-Doherty Earth Observatory, Columbia University, New York, NY, USA, [4]State Key Laboratory of Tropical Oceanography, South China Sea Institute of Oceanology, Chinese Academy of Sciences, Beijing, China, [5]Physical Sciences Laboratory, NOAA Earth System Research Laboratories, Boulder, CO, USA, [6]NASA Goddard Institute for Space Studies, Greenbelt, MD, USA, [7]Center for Climate Systems Research, Earth Institute, Columbia University, New York, NY, USA, [8]Department of Geosciences, Princeton University, Princeton, NJ, USA, [9]The High Meadows Environmental Institute, Princeton University, Princeton, NJ, USA, [10]Department of Earth System Science, University of California Irvine, Irvine, CA, USA, [11]Earth Observatory of Singapore, Nanyang Technological University, Singapore, Singapore

Key Points:

- ColdBlobMIP shows that the North Atlantic warming hole causes small but robust changes in surface winds, sea level pressure, and clouds
- Cloud feedbacks may amplify cooling, with a shortwave forcing of −3.6 W/m^2 in summer from increased cloud cover
- Despite a common sea surface temperatures forcing, models show three distinct atmospheric responses, revealing diverse underlying physical mechanisms

Supporting Information:

Supporting Information may be found in the online version of this article.

Correspondence to:

K. B. Karnauskas,
kristopher.karnauskas@colorado.edu

Citation:

Kramer, S. M., Karnauskas, K. B., Elling, M. T., Zhang, L., Liu, H., Chen, Y., et al. (2025). ColdBlobMIP: A multi-model assessment of the atmospheric response to the North Atlantic warming hole. *Geophysical Research Letters*, *52*, e2025GL117784. https://doi.org/10.1029/2025GL117784

Received 23 JUN 2025
Accepted 15 SEP 2025

Author Contributions:

Conceptualization: Sydney M. Kramer, Kristopher B. Karnauskas
Data curation: Sydney M. Kramer, Kristopher B. Karnauskas
Formal analysis: Sydney M. Kramer, Kristopher B. Karnauskas, Maxwell T. Elling, Lei Zhang, Heng Liu, Yanying Chen, Dillon J. Amaya, Larissa Nazarenko, Wenchang Yang, Dervla Meegan-Kumar
Funding acquisition: Kristopher B. Karnauskas

Abstract Observations of sea surface temperature reveal a region of relative cooling in the subpolar North Atlantic commonly known as the North Atlantic warming hole (NAWH) or "cold blob." While the origin of the NAWH has been extensively debated, its direct impact on the atmosphere has only recently garnered attention. Here, we present ColdBlobMIP, an atmospheric model intercomparison project in which 15 models from four institutions simulate the atmospheric response to the observed NAWH. The ensemble mean reveals robust and significant changes in surface wind and clouds, the latter imparting a shortwave forcing of −3.6 W/m^2 over the NAWH in summer—indicative of a positive feedback. Despite agreement on certain aspects of the response, the models exhibit diverse behavior that is diagnosed from their surface pressure response. Overall, ColdBlobMIP attributes a relatively modest response to the NAWH, highlighting the critical dependence of large-scale midlatitude air-sea interactions on model structure and configuration.

Plain Language Summary In a world of rising ocean temperatures, one area in the North Atlantic stands out for bucking the trend: a persistent patch of cooling known as the "cold blob," located south of Greenland. Scientists have debated what causes it, but its impact on the atmosphere above has remained unclear. A new study called ColdBlobMIP brought together 15 different climate models to investigate how this cold blob influences surface winds, air pressure, and clouds. The models agree that the cold blob leads to significant shifts in wintertime wind patterns and an increase in summertime cloud cover, which could reinforce the cooling by blocking sunlight. However, the study also finds that different models produce different patterns of atmospheric response, suggesting that how a model is built plays an important role in how the atmosphere reacts to the cold blob. The findings highlight both the subtle but real effects of regional ocean cooling on the atmosphere, and the importance of using multiple models to understand how these interactions play out in the climate system.

1. Introduction

While global sea surface temperatures (SST) have risen by an average of 0.55°C since 1970 due to anthropogenic forcing (Collins et al., 2013), a region south of Greenland—the North Atlantic Warming Hole (NAWH)—has cooled by ∼0.5°C since 1870 (Figure 1a). This feature, also called the "cold blob," appears consistently across observations and coupled model simulations of both historical and future climates (Dagan et al., 2020), indicating a robust response to external forcing. Despite strong model agreement on its persistence, the atmospheric response to the NAWH varies across simulations (Geng et al., 2025; Gervais et al., 2019; Grist et al., 2025; Hall et al., 2001; Karnauskas et al., 2021; Kramer et al., 2024). This study aims to understand the steady-state atmospheric response to the observed NAWH using a broader suite of models.

The NAWH is widely attributed to a buoyancy-driven weakening of the Atlantic Meridional Overturning Circulation (AMOC) (e.g., Caesar et al., 2018; K. Y. Li & Liu, 2025; X. Li et al., 2025; Rahmstorf et al., 2015),

Investigation: Sydney M. Kramer, Kristopher B. Karnauskas, Dhrubajyoti Samanta
Methodology: Sydney M. Kramer, Kristopher B. Karnauskas
Project administration: Kristopher B. Karnauskas
Resources: Kristopher B. Karnauskas, Lei Zhang, Gabriel A. Vecchi, Jane W. Baldwin
Software: Sydney M. Kramer, Kristopher B. Karnauskas
Supervision: Kristopher B. Karnauskas
Validation: Sydney M. Kramer, Kristopher B. Karnauskas
Visualization: Sydney M. Kramer, Kristopher B. Karnauskas
Writing – original draft: Sydney M. Kramer, Kristopher B. Karnauskas
Writing – review & editing: Sydney M. Kramer, Kristopher B. Karnauskas, Maxwell T. Elling, Lei Zhang, Dillon J. Amaya, Wenchang Yang, Gabriel A. Vecchi, Dervla Meegan-Kumar, Jane W. Baldwin, Dhrubajyoti Samanta

although direct confirmation of long-term AMOC weakening remains elusive (Smeed et al., 2014). Other mechanisms—including air-sea interaction, subpolar gyre variability, local mixing, shortwave cloud feedbacks, remote teleconnections, and storminess—have also been implicated (e.g., Hu & Fedorov, 2020; Keil et al., 2020; L. Li et al., 2022; Mackay et al., 2024). Our study does not explicitly test these mechanisms concerning the formation of the NAWH but instead seeks to isolate its present impact on the atmosphere including potential feedbacks.

To do so, we employ an atmospheric model intercomparison project (AMIP)-style framework in which multiple atmospheric general circulation models (AGCMs) are forced with consistent SST boundary conditions (Gates et al., 1999). While this setup sacrifices interactive coupling (e.g., Covey et al., 2003), it allows for efficient comparison of responses across models and isolation of forcing uncertainty. Such intercomparisons—from AMIP1 to the recent Tropical Basin Interaction Model Intercomparison Project (TBIMIP, Richter et al., 2025)—are essential tools for diagnosing model behavior, identifying systematic errors, and quantifying uncertainties in the physical response of the atmosphere to different patterns of ocean forcing. Our effort, ColdBlobMIP, is an ad hoc intercomparison involving 15 AGCM configurations from nine base models across four institutions, designed to understand the atmospheric imprint of the NAWH.

In this study, we focus on sea level pressure (SLP), surface wind and vertically integrated total cloud cover. In addition to providing useful insight into the dominant physical mechanism shaping the atmospheric response to SST forcing, SLP is an imprecise yet useful diagnostic of surface winds through geostrophy. We analyze changes in surface wind speed and clouds because they modulate latent heat flux and shortwave radiation, respectively, and are therefore central to potential feedbacks on SST.

The following section describes the collection of models used, experimental design and criteria for evaluating significance. In Section 3, we evaluate the multi-model ensemble mean results while also examining the diversity of patterns and mechanisms across the models. Finally, Section 4 gives a summary and places the results in a broader context.

2. Methodology

2.1. Participating Models

Atmospheric general circulation models (AGCMs) developed at four different institutions are included in this study: the Max Planck Institute in Germany, the U.S. National Center for Atmospheric Research (NCAR), the U.S. NOAA Geophysical Fluid Dynamics Laboratory (GFDL), and the U.S. NASA Goddard Institute for Space Studies (GISS); see Tables 1 and Table S1 in Supporting Information S1 for relevant model attributes and acronym definitions. These models span a range of vintages (e.g., NCAR-CAM4 through CAM6), horizontal resolutions (from 50 km to ∼3°) and vertical resolutions (from 19 to 110 vertical levels). We also ran an identical model and configuration (NCAR-CAM6-BGC) on two different supercomputers (labeled 7 and 9 in Table 1) to test the sensitivity of our results to computer architecture and system-level software.

Nine distinct base models of AGCMs are used (MPI-ECHAM4.6, NCAR-CAM4/5/6, GFDL-AM2.1/2.5 and HiRAM, and GISS-ModelE2.1/3). Some of these AGCMs were run with varying horizontal resolution, atmospheric chemistry, and land surface schemes, ultimately yielding a total of 15 unique model configurations running the same experiment (Table 1). For brevity, we hereafter refer to all 15 of these configurations as "models." The outputs of each model were linearly regridded to a common 1° grid for comparison. Note that cloud cover is only available for 10 of the 15 participating models (not saved or recoverable from models numbered 1, 2, 7, 8, and 10 in Table 1).

The simulations using MPI-ECHAM4.6-T42 and NCAR-CAM6-BGC (run on the NCAR Cheyenne supercomputer) are described in Karnauskas et al. (2021) and Kramer et al. (2024), respectively. Otherwise, this so-called MIP-style experiment was conducted on an ad hoc basis by the coauthors of this study, as opposed to the more formal MIP frameworks organized by the World Climate Research Programme. Put simply, these models are routinely run by a group of informal collaborators who volunteered to contribute to this experiment.

10.1029/2025GL117784

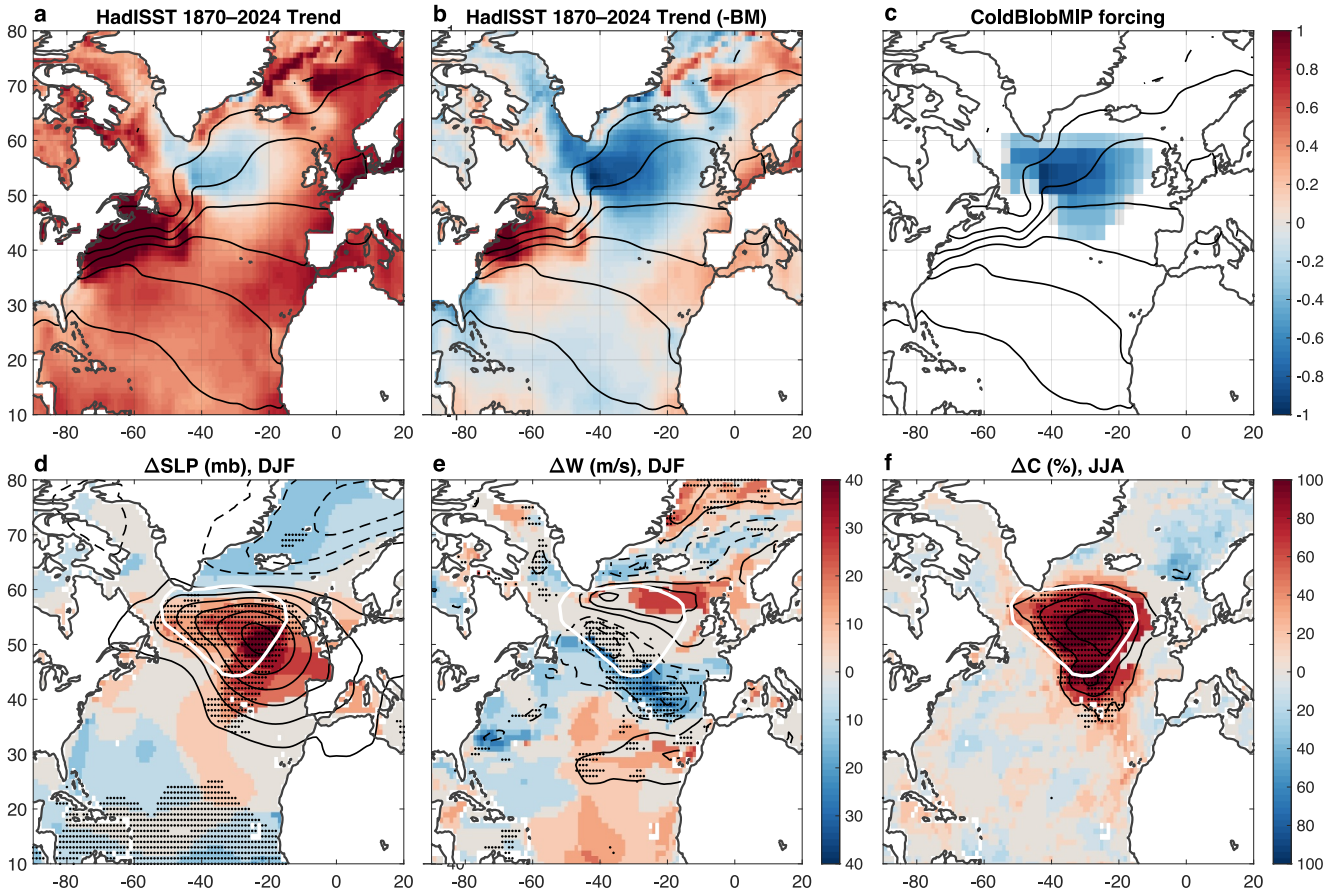

Figure 1. (a) Observed sea surface temperatures (SST) trend (°C per century) over 1870–2024 from the HadISST data set. (b) As in (a) but with the basin mean removed (0.52°C per century, calculated from 55°S to 60°N). (c) SST anomaly (°C) added to prescribed climatology in each model to construct the "cold blob" SST forcing. The field in panel (c) is displayed after interpolation onto the T42 grid of the first model listed in Table 1. For context, panels (a–c) include the time-mean SST field (black contours, interval 4°C, HadISST). (d) Multi-model mean boreal winter (DJF) sea level pressure (SLP) response (cold blob minus control) (black contours, interval 0.1 mb, dashed negative, zero omitted). Colors indicate the percentage of models that yield a statistically significant difference between the DJF mean SLP field in the cold blob and control simulation in each grid cell (two-tailed Student's *t*-test, $\alpha = 0.1$, red and blue for models with positive and negative change, respectively). Black dots indicate grid cells where at least 75% of the 15 models agree on the sign of change. Thick white contour marks the general location of the cold blob SST forcing (−0.33°C isotherm plotted). (e) As in (d) but for wind speed (interval 0.05 m/s, zero omitted). (f) As in (d) but for boreal summer (JJA) cloud cover (interval 0.5%). Note that the same color scale applies to panels (d, e) (ranging from 40% of models have a statistically significant negative response to 40% of models have a statistically significant positive response), while (f) has a different color scale (100% negative to 100% positive), and cloud cover was only available for 10 models (i.e., 100% in panel (c) means 10/10 models). The intermodel agreement threshold in panel (f) is also different than in panels (d, e)—black dots in panel (c) indicate 100% of models agree on the sign of cloud cover change. See Figure S5 in Supporting Information S1 for the SLP response in JJA and cloud response in DJF.

2.2. Forcing and Experimental Design

The simulations span a minimum of 40 years up to 201 years (Table 1). In calculating seasonal climatologies, we discarded the first 3 years of output from each simulation to account for model adjustment to the prescribed SST forcing ("spinup"). SST boundary conditions were prescribed as a repeating 12-month climatology. SST climatologies do vary subtly between simulations—due to differences in the observational product and time ranges used by each institution to compute each climatology (Table 1)—as a result of our decision to leverage existing AGCM simulations to serve as control cases. We note that differences between model solutions to the same SST forcing are much larger than differences between climatological observations averaged over the different periods (Figures S1a–S1d vs. Figure S1e in Supporting Information S1).

To construct the "cold blob" SST boundary condition, a cold SST anomaly in the subpolar North Atlantic was added to each model's respective control climatology (hereafter referred to as the cold blob SST forcing). The cold blob SST forcing used is identical to that of Karnauskas et al. (2021) and Kramer et al. (2024). Karnauskas et al. (2021) constructed this forcing by isolating the NAWH in the basin-relative SST trend from HadISST

Table 1
List of 15 Models or Model Configurations Used in the Present Study Including Institution, Vintage or Common Name, Version, Grid, Horizontal Resolution (Longitude by Latitude, or km for the C180 Cubed-Sphere Grid), Number of Vertical Levels, Land Surface Model or Vegetation Prescription, Number of Years Included in Experiment, Information on the Prescribed Sea Surface Temperatures Climatology (Source and Period), and Computer Used to Run the Experiment

No.	Inst.	Vintage	Version	Grid	Resolution	Lev.	Land/veg.	Years	SST clim.	SST period	Machine	Mech.
1	MPI	ECHAM	4.6	T42	2.81° × 2.79°	19	Prescribed	40	OIv2	1982–2019	Indopac	A
2				T106	1.13° × 1.12°	19	Prescribed	42	OIv2	1982–2019	Indopac	C
3	NCAR	CESM1	CAM4	F25	3.33° × 2.54°	26	SP	200	Hurrell08	1995–2005	SCSIO	A
4				F09	1.25° × 0.94°	26	SP	200	Hurrell08	1995–2005	SCSIO	C
5			CAM5	F25	3.33° × 2.54°	30	SP	200	Hurrell08	1995–2005	SCSIO	C
6				F09	1.25° × 0.94°	30	SP	200	Hurrell08	1995–2005	SCSIO	A
7		CESM2	CAM6	F09	1.25° × 0.94°	32	BGC	50	Hurrell08	1995–2005	Cheyenne	B
8							SP	55	Hurrell08	1995–2005	Derecho	B
9							BGC	200	Hurrell08	1995–2005	Derecho	C
10	GFDL	CM2.1	AM2.1	Arakawa B	2.50° × 2.02°	24	Prescribed	40	OIv2	1982–2019	Cheyenne	B
11		CM2.5	AM2.5	FV3 C180	50 km	32	LM3	200	Hurrell08	1986–2005	Tiger	C
12		HiRAM		FV3 C180	50 km	32	LM3	200	Hurrell08	1986–2005	Tiger	A
13	GISS	ModelE2.1	NINT	Gridpoint	2.50° × 2.00°	40	ENT	201	Hurrell08	1995–2005	Discover	B
14			OMA	Gridpoint	2.50° × 2.00°	40	ENT	201	Hurrell08	1995–2005	Discover	A
15		ModelE3	MATRIX	Gridpoint	2.50° × 2.00°	110	ENT	200	HadISST	2003–2017	Discover	B

Note. Letters A–C in the final column indicate the dominant physical mechanism diagnosed by the latitudinal gradient of SLP response (P'_y) in the vicinity of the cold blob; see main text, Figure 2 and Figure S9 in Supporting Information S1 for details. See main text and Table S1 in Supporting Information S1 for definitions of acronyms used in this table. References for OIv2 and Hurrell08 SST data are Huang et al. (2021) and Hurrell et al. (2008), respectively.

(Rayner et al., 2003) over the period 1870–2019. The basin-relative trend over the period extending through 2024 is virtually indistinguishable from that ending in 2019 and remains well represented by the cold blob SST forcing (Figure 1b). This anomaly was applied uniformly to each month of the climatology—observations of the SST trend do not justify a more complex approach, such as a seasonally varying amplitude or spatial pattern of the cold blob SST forcing (Figure S2 in Supporting Information S1).

2.3. Evaluation of Significance

We evaluate the significance of the atmospheric response to cold blob SST forcing from four distinct perspectives: *statistical* significance, uncertainty or *robustness*, *physical* significance, and *technical* significance.

For each model, we evaluate the statistical significance of the response by performing a two-tailed Student's *t*-test for differences in the mean (using $\alpha = 0.1$, equivalent to a 90% confidence limit). Such tests are conducted after taking seasonal means of the monthly, regridded outputs (boreal winter and summer). To convey the geographic variation of statistically significant responses (or lack thereof) amongst the models, we additionally map the percentage of models that exhibited a significant response at each grid cell. In the event of a conflict—that is, grid cells where different models yield both significant positive and significant negative responses—the percentage for that grid cell is set to zero (Figures 1d–1f).

Independent of the statistical significance of the atmospheric response to cold blob SST forcing in each model, the robustness of the multi-model mean result is evaluated as the number of models that agree on the sign of change in each grid cell. For simplicity, criteria such as 75% or 100% are chosen, and when those criteria are met in a given grid cell for a particular variable, a small black dot is applied (Figures 1d–1f).

It is reasonable to predict that the midlatitude, steady-state atmospheric response to an SST anomaly with a peak as modest as −1°C may be small. In addition to evaluating robustness and statistical significance, we evaluate the *physical* significance of the response in terms of the extent to which it could contribute meaningfully to changes in the prescribed forcing; that is, are they a substantial feedback on SST? The physical significance of the simulated response of both wind speed and clouds is therefore evaluated by estimating their implications for surface fluxes

via bulk formulas, and then for SST tendency (i.e., feedbacks on the cold blob SST forcing) via an ocean mixed layer heat budget. The latent heat flux anomaly due to a simulated surface wind speed response is calculated as

$$Q_{\mathrm{LH}}{}' = \rho_a \, L_v \, C_{\mathrm{LH}} \, W' \, \Delta q \tag{1}$$

where $Q_{\mathrm{LH}}{}'$ is the latent heat flux anomaly (W m^{-2}), ρ_a is reference air density (1.3 kg m^{-3}), L_v is the latent heat of vaporization (2.3×10^6 J kg^{-1}), C_{LH} is transfer coefficient for latent heat (1.2×10^{-3}), W' is the near-surface wind speed response (taken from model output), and Δq is the near-surface specific humidity gradient (2 g kg^{-1}, estimated from observations). The surface shortwave flux anomaly due to a simulated cloud cover response is calculated as

$$Q_{\mathrm{SW}}{}' = \lambda \, C' \tag{2}$$

where $Q_{\mathrm{SW}}{}'$ is the surface shortwave radiation anomaly (in W m^{-2}), λ is the cloud shortwave forcing, and C' is the cloud cover response (taken from model output). λ is known to vary widely based on region, season and cloud type (Key & Minnett, 2006; Poetzsch-Heffter et al., 1995); we therefore calculated it for the subpolar North Atlantic region and season using ERA5 (Hersbach et al., 2020); a value of -237 ± 20 W/m^2 per unit cloud cover was obtained (Figure S3 in Supporting Information S1).

Next, the impact of these fluxes on SST tendency is calculated as

$$T_t = \frac{Q'}{\rho_o \, C_p \, h} \tag{3}$$

where T_t is the SST tendency (expressed in °C per decade), Q' is either $Q_{\mathrm{LH}}{}'$ or $Q_{\mathrm{SW}}{}'$ from Equation 1 or Equation 2, respectively, ρ_o is reference seawater density (1,025 kg m^{-3}), C_p is the specific heat capacity of seawater (3,850 J kg^{-1} K^{-1}), and h is the mixed layer depth. The observed seasonal mean mixed layer depth (de Boyer Montégut et al., 2004) averaged within the cold blob SST forcing is used (168 m for DJF and 25 m for JJA, Figure S4 in Supporting Information S1). From the sign and magnitude of T_t, we can infer the physical significance of the atmospheric response to cold blob SST forcing, including whether it may contribute to important feedbacks on the NAWH.

Finally, we consider whether the impact of the cold blob SST forcing on the time-mean atmosphere is significant relative to that of other differences in model attributes. To do so, we assess how much the climatological means of SLP, wind and clouds over the subpolar North Atlantic varies amongst the control simulations of the models. These considerations are presented in the following section as a measure of so-called "technical" significance.

3. Results

3.1. Multi-Model Mean and Significance

The multi-model mean boreal winter atmospheric response to cold blob SST forcing is defined by an anticyclone with SLP amplitude ~0.6 mb roughly collocated with the NAWH (albeit centered slightly to the southeast) and a −0.3 mb cyclonic anomaly to the northeast of the cold blob centered over the Greenland and Norwegian Seas (Figure 1d). The multi-model mean SLP response is robust, with at least 75% of the models agreeing on the sign of change over the center and western half of the anticyclone and a small portion of the cyclonic response just north of Iceland. Relative to each model's internal variability, 40% exhibit a statistically significant change at the center of the anticyclone.

Consistent with the SLP response, the multi-model mean boreal winter surface wind speed response features an approximately symmetric dipole of positive and negative wind speed anomalies along the northern and southern margins of the anticyclonic response, respectively, with amplitude ±0.15 m/s (Figure 1e). A slightly weaker dipole of wind speed anomalies is also found along the northern and southern fringes of the cyclonic anomaly over the Greenland and Norwegian Seas. An acceleration along the northern margin of the anticyclonic response is statistically significant in 27% (4/15) of models and a deceleration along the southern margin is statistically significant in 33% (5/15) of models. Only the multi-model mean deceleration along the southern margin of the

anticyclone and the acceleration along the northern margin of the cyclone are robust (75% of models). The atmospheric circulation response during boreal summer is qualitatively similar but roughly one third as strong (Figure S5 in Supporting Information S1).

In contrast to SLP and wind, the response of cloud cover to cold blob SST forcing is most prominent in boreal summer (Figures S5 and S6 in Supporting Information S1). Although the multi-model mean boreal summer cloud response is relatively small (∼1.5%), it is highly statistically significant and robust. All 10 of the models that provided cloud cover output exhibit a statistically significant increase in cloud cover directly over the NAWH and, naturally, 100% of the models agree on the sign of change there (Figure 1f). This response is physically consistent with established boundary-layer cloud dynamics. Colder SSTs, particularly in the midlatitudes, promote the formation of low-level marine stratus and stratocumulus clouds by enhancing lower-tropospheric stability and suppressing vertical mixing between the moist boundary layer and the drier free troposphere. Using the model from which we have both vertically integrated total cloud cover and cloud cover on multiple levels, it is clear that the response is entirely at low levels (Figure S7 in Supporting Information S1).

Overall, the multi-model mean atmospheric response to cold blob SST forcing is relatively small in magnitude relative to the background levels—about 0.6 mb SLP, 0.15 m/s wind speed and 1.5% cloud cover. Several of the salient features are robust across the multi-model ensemble and emerge as statistically significant within several models. What is the physical significance of this response, particularly in terms of feedbacks? Invoking Equations 1 and 3, a wind speed change of ±0.15 m/s yields a latent heat flux change of ±1.1 W/m^2 and an SST tendency of ±0.004°C per month—or ±0.126°C per decade if operating for only 3 months per year (DJF). This represents a negative feedback on the cold SST trend along the southern margin of the NAWH (wind deceleration) and a positive feedback along the northern margin of the NAWH (wind acceleration). Shifting to the cloud response and invoking Equations 2 and 3, a cloud cover increase of 1.5% yields a surface shortwave flux reduction of −3.6 W/m^2 and an SST tendency of −0.093°C per month—or −2.802°C per decade if operating for only 3 months per year (JJA). As with wind-evaporation, this cloud-shortwave feedback is of physical significance relative to the total observed SST trend defining the NAWH (Figures 1a–1c) but considerably stronger. Overall, these two feedbacks would render the cold blob stronger and centered slightly further north than it otherwise would be. While outside the scope of this study, other physical processes associated with the multi-model mean atmospheric response such as upper ocean mixing, which can be modulated by wind speed, may introduce additional feedbacks via latent heat flux and/or changes in the mixed layer depth that are qualitatively consistent with that of latent heat flux.

A last point of comparison for the multi-model mean atmospheric response to cold blob SST forcing is the extent to which the mean climatology of the variables examined here within the subpolar North Atlantic is sensitive to model, and even different configurations of a single model. As motivated in Section 2.2, this is neither a measure of statistical significance, robustness, nor physical significance—but something of a technical significance. At the latitude of the peak SLP anomaly (51°N), there is a 9.6-mb spread in the climatological SLP magnitude across the 15 control simulations (Figure S8a in Supporting Information S1), or 16 times the amplitude of the peak SLP response in the cold blob simulations (0.6 mb). In other words, differences between models and model configurations have a much larger impact on the simulated SLP over the subpolar North Atlantic than does the observed cold blob. Similar results are obtained for wind speed and cloud cover (Figures S8b and S8c in Supporting Information S1), which vary across the models at relevant latitudes by ∼3.8 m/s and 18.5%, respectively—both well over 10 times the multi-model mean response to cold blob SST forcing.

3.2. Diversity of Patterns and Mechanisms

Although the multi-model mean SLP response features some significant and robust features, such as an anticyclone roughly collocated with the NAWH, it is worth examining the diversity of the spatial patterns across the 15 models participating in ColdBlobMIP and the implications for the physical mechanism(s) governing their individual responses. In the MPI-ECHAM4.6-T42 experiment (model 1), the mechanism diagnosed by Karnauskas et al. (2021) involved an increase in stability over the cold blob decelerating the climatological westerlies (Hayes et al., 1989; Wallace et al., 1989) with a concomitant geostrophic adjustment (Rossby, 1938) toward higher (lower) SLP to the north (south) of the cold blob (Figure 2a; see also Kramer (2025) and Figure S9a in Supporting Information S1 for schematic). We identify this mechanism (hereafter referred to as mechanism "A") in the models by a positive slope of the zonal mean profile of SLP response (P'_y) at the central latitude of the

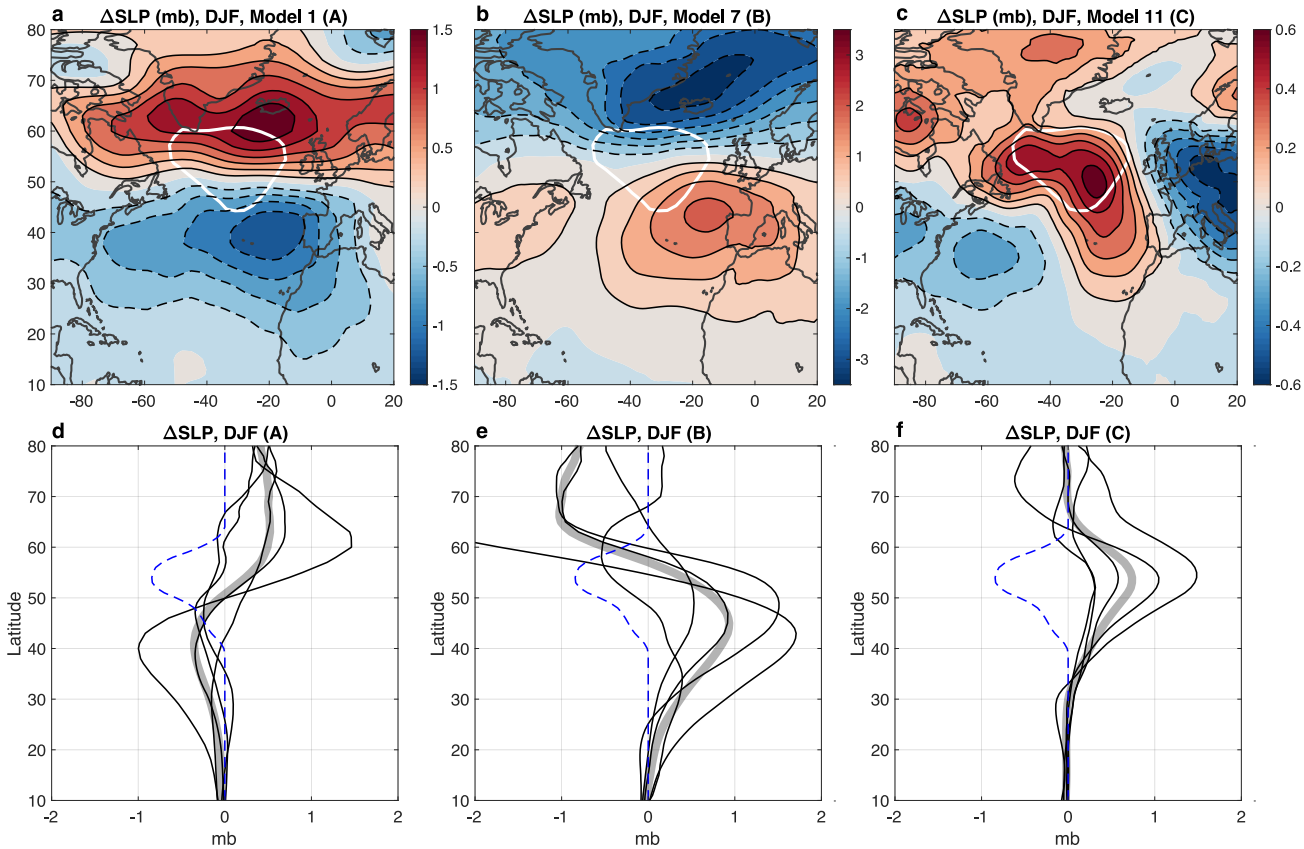

Figure 2. Boreal winter (DJF) sea level pressure (SLP) response (mb) in three models that exemplify the three categories of dominant physical mechanisms shaping the response: (a) model 1 (MPI-ECHAM4.6-T42) for mechanism A, (b) model 7 (NCAR-CAM6-BGC/Cheyenne) for mechanism B, and (c) model 11 (GFDL-CM2.5) for mechanism C. Thick white contour in panels (a–c) marks the general location of the cold blob sea surface temperatures (SST) forcing (−0.33°C isotherm plotted). The contour intervals in panels (a–c) are 0.25, 0.5, and 0.1 mb, respectively, with dashed negative and zero omitted. (d) Zonal mean SLP profiles (45°W–0°W) of the 5 models diagnosed as mechanism A (thin black lines), along with the mean of those five models (thick gray line), and the SST forcing zonally averaged through the center of the cold blob (44°W–26°W) (blue dashed line). (e, f) As in (a) but for mechanisms B and C, respectively. For two models in panel (d) (3 and 6), the eastern limit of the zonal mean is set to 35°W to accommodate the zonal offset in their pattern relative to the other "A" models).

cold blob SST forcing. Besides the aforementioned MPI-ECHAM4.6, four other models share this pattern including models from NCAR, GFDL, and GISS (Figure 2d and Table 1). Moreover, in the NCAR-CAM6-BGC run on the Cheyenne supercomputer, a roughly opposite pattern emerges as a nonlinear equivalent barotropic response to SST forcing. In this case, known as the transient eddy forced response, the enhancement of the meridional SST gradient in the subpolar North Atlantic by the cold blob strengthens transient eddies that propagate vertically and enhance the midlatitude jet, resulting in the SLP dipole evident in Figure 2b (Gervais et al., 2019; Kramer et al., 2024) (see also Kramer (2025) and Figure S9b in Supporting Information S1 for schematic). Likewise, four additional models share this pattern (hereafter referred to as mechanism "B") as diagnosed by a negative P'_y across the cold blob (Figure 2e).

Remarkably, the five remaining models not captured by mechanism A or B by way of the sign of P'_y across the cold blob all have an extremely consistent pattern: a positive peak in SLP anomaly that is closely aligned with the center of the cold blob SST forcing (i.e., $P'_y = 0$ there) as shown in Figure 2f and exemplified by model 11 (Figure 2c). We suggest that the response in the five models included in this third category (hereafter referred to as mechanism "C") is dominated by the well-mixed boundary layer adjustment of (hydrostatic) pressure to the cold SST (Lindzen & Nigam, 1987; see also Kramer (2025) and Figure S9c in Supporting Information S1 for a schematic). A similar mechanism was also described as a direct linear response by Gervais et al. (2019); see Gervais et al. (2019) for an excellent discussion of this and mechanism B. Other statistical methods for pattern-based classification are available; k-means clustering, for example, yields very similar results (confirming that 3 is the optimal number of clusters, and agreeing with our criterion on 13 of 15 models). The two models upon

which the two methods disagree are where the P'_y criterion identified mechanism B and k-means clustering identified mechanism C. Where k-means disagrees, it is clear from visual inspection that the latitudinal structure of the SLP response near the central latitude of the cold blob SST forcing was not a priority.

The multi-model mean boreal winter SLP response is a residual average of three relatively easily distinguishable categories of model responses and associated dominant mechanism (coincidentally, with 5 models apiece). Given that mechanisms A and B are roughly opposites, it is natural that there be some cancellation, leaving the multi-model mean of all 15 models to most closely resemble mechanism C. That the multi-model mean SLP response has a slight southward bias of the anticyclone otherwise collocated with the cold blob is due to the average of the five models in mechanism B (with the high SLP anomaly located to the south of the cold blob) being stronger in magnitude than that for mechanism A (with the high SLP anomaly located to the north of the cold blob) (c.f. Figures 2d and 2e). Moreover, since mechanisms A and B are not perfectly symmetric (A is shifted slightly southward and B is shifted slightly northward), there is a ∼6°-wide range of latitude in which the three category-mean response profiles are positive (Figure S10 in Supporting Information S1), which explains why there is strong multi-model agreement in the high SLP response over the center of the cold blob SST forcing. The three physical mechanisms (A-C) are not mutually exclusive, of course. There is undoubtedly a mixture of mechanisms at play, even if one of them dominates in a given model. It appears that models categorized as A or B have some measure of mechanism C, which would explain why the high SLP feature of their category-mean profiles is biased toward the cold blob SST forcing.

4. Discussion and Conclusions

In this study, we introduced ColdBlobMIP—a focused, ad hoc model intercomparison project designed to assess the atmospheric response to the observed NAWH, or cold blob. Using 15 configurations of nine AGCMs from four institutions, we imposed a realistic SST anomaly based on observed trends and evaluated the resulting changes in SLP, surface wind speed, and cloud cover. Our approach assessed not only the ensemble mean response, but also its statistical, physical, and technical significance.

Despite the relatively modest amplitude of the SST forcing (peaking at ∼−1°C), some robust and significant features emerge in the multi-model mean response. In boreal winter, a weak but coherent anticyclone emerges over the cold blob, flanked by compensating cyclonic anomalies. This pattern is echoed in the surface wind field, featuring a dipole of acceleration/deceleration consistent with geostrophic adjustment. In boreal summer, the atmospheric response is dominated by a robust and statistically significant increase (∼1.5%) in low-level cloudiness directly over the cold SSTs, implying enhanced boundary-layer stability and suppressed vertical mixing.

These changes, though small in magnitude, yield surface energy flux anomalies that would act as consequential feedbacks on the imposed SST perturbations—that is, they are *physically* significant. Simple bulk formulations suggest a latent heat flux feedback of ±1.1 W/m^2 from wintertime wind anomalies and a much larger shortwave feedback of −3.6 W/m^2 from summertime cloud cover anomalies. When propagated through the ocean mixed layer, these imply SST tendencies of up to ±0.13°C/decade (wind) and −2.8°C/decade (clouds)—on par with or larger than the historical cold blob trend itself, suggesting some ocean adjustment that is dampening the SST response to these inferred flux anomalies.

As the NAWH is a relatively weak mid-high latitude SST anomaly embedded within a region of strong internal atmospheric variability, the associated atmospheric response is a "needle in a haystack," yet ColdBlobMIP was able to clarify its essential features and implications. It is important to recall the diversity of model responses; the multi-model mean is largely shaped by a residual between three distinct patterns. It should also be borne in mind that our estimates of feedback magnitudes in Section 3.1 are simple back-of-the-envelope calculations meant to contextualize the simulated response but indeed imply some physical significance to the real climate system, especially via clouds and shortwave radiation. That the atmospheric response to the observed NAWH is relatively small compared to intermodel differences in climatology may be unsurprising to model developers; the direct comparison nonetheless represents a unique contextualization of model biases. ColdBlobMIP underscores that, while computational resources and technical skills are often a limiting factor, testing the robustness of results across different model configurations is important whenever possible.

Conflict of Interest

The authors declare no conflicts of interest relevant to this study.

Data Availability Statement

All model outputs required to reproduce the analyses presented in this paper are archived and documented on Zenodo via Kramer and Karnauskas (2025). Any other outputs may be provided upon reasonable request to the corresponding author. All observational data used are publicly accessible:

ERA5: https://www.ecmwf.int/en/forecasts/dataset/ecmwf-reanalysis-v5
HadISST: https://www.metoffice.gov.uk/hadobs/hadisst/
IFREMER mixed layer depth climatology: https://cerweb.ifremer.fr/deboyer/mld/Data.php

Acknowledgments
J. W. B. and D. M. K. were supported by the NASA New Investigator Program in Earth Science (80NSSC21K1735). W. Y. and G. A. V. are supported in part by the Heising-Simons Foundation. S. M. K. and K. B. K. acknowledge high-performance computing support from the Cheyenne (doi: 10.5065/D6RX99HX) and Derecho (doi: 10.5065/qx9a-pg09) systems provided by the NSF-sponsored National Center for Atmospheric Research. Some of the numerical simulations conducted by L. Z., H. L., and Y. C. were supported by the High-Performance Computing Division of the South China Sea Institute of Oceanology. The authors acknowledge Dr. Maria Gehne for conducting an internal review of the manuscript prior to submission.

References

Caesar, L., Rahmstorf, S., Robinson, A., Feulner, G., & Saba, V. (2018). Observed fingerprint of a weakening Atlantic Ocean overturning circulation. *Nature*, *556*(77007700), 191–196. https://doi.org/10.1038/s41586-018-0006-5

Collins, M., Knutti, R., Arblaster, J., Dufresne, J. L., Fichefet, T., Friedlingstein, P., et al. (2013). Long-term climate change: Projections, commitments and irreversibility. In T. F. Stocker, D. Qin, G.-K. Plattner, M. Tignor, S. K. Allen, J. Boschung, et al. (Eds.), *Climate change 2013: The physical science basis. Contribution of working group I to the fifth assessment report of the intergovernmental panel on climate change* (pp. 1029–1136). Cambridge University Press.

Covey, C., AchutaRao, K. M., Cubasch, U., Jones, P., Lambert, S. J., Mann, M. E., et al. (2003). An overview of results from the coupled model intercomparison project. *Global and Planetary Change*, *37*(1–2), 103–133. https://doi.org/10.1016/s0921-8181(02)00193-5

Dagan, G., Stier, P., & Watson-Parris, D. (2020). Aerosol forcing masks and delays the formation of the North Atlantic warming hole by three decades. *Geophysical Research Letters*, *47*(22), e2020GL090778. https://doi.org/10.1029/2020GL090778

de Boyer Montégut, C., Madec, G., Fischer, A. S., Lazar, A., & Iudicone, D. (2004). Mixed layer depth over the global ocean: An examination of profile data and a profile-based climatology. *Journal of Geophysical Research*, *109*, C12003. https://doi.org/10.1029/2004JC002378

Gates, W. L., Boyle, J. S., Covey, C., Dease, C. G., Doutriaux, C. M., Drach, R. S., et al. (1999). An overview of the results of the atmospheric model intercomparison project (AMIP I). *Bulletin of the American Meteorological Society*, *80*(1), 29–55. https://doi.org/10.1175/1520-0477(1999)080<0029:aootro>2.0.co;2

Geng, X., Oh, J., Shin, Y., Shin, J., Noh, K., Park, S., & Kug, J. (2025). Non-monotonic future changes in the north Atlantic warming hole under a fast CO_2 emission scenario. *Journal of Climate*. https://doi.org/10.1175/JCLI-D-24-0437.1

Gervais, M., Shaman, J., & Kushnir, Y. (2019). Impacts of the North Atlantic warming hole in future climate projections: Mean atmospheric circulation and the North Atlantic jet. *Journal of Climate*, *32*(10), 2673–2689. https://doi.org/10.1175/JCLI-D-18-0647.1

Grist, J. P., Josey, S. A., Sinha, B., Screen, J. A., Marsh, R., & Dey, D. (2025). The impact of a subpolar North Atlantic freshwater anomaly on Eurasian winter climate. *Journal of Climate*. https://doi.org/10.1175/JCLI-D-24-0669.1

Hall, N. M., Lin, H., & Derome, J. (2001). The extratropical signal generated by a midlatitude SST anomaly. Part II: Influence on seasonal forecasts. *Journal of Climate*, *14*(12), 2696–2709. https://doi.org/10.1175/1520-0442(2001)014,2696:TESGBA.2.0.CO;2

Hayes, S., McPhaden, M., & Wallace, J. (1989). The influence of sea-surface temperature on surface wind in the eastern equatorial Pacific: Weekly to monthly variability. *Journal of Climate*, *2*(12), 1500–1506. https://doi.org/10.1175/1520-0442(1989)002<1500:tiosst>2.0.co;2

Hersbach, H., Bell, B., Berrisford, P., Hirahara, S., Horányi, A., Muñoz-Sabater, J., et al. (2020). The ERA5 global reanalysis. *Quarterly Journal of the Royal Meteorological Society*, *146*(730), 1999–2049. https://doi.org/10.1002/qj.3803

Hu, S., & Fedorov, A. V. (2020). Indian Ocean warming as a driver of the North Atlantic warming hole. *Nature Communications*, *11*(11), 4785. https://doi.org/10.1038/s41467-020-18522-5

Huang, B., Liu, C., Banzon, V., Freeman, E., Graham, G., Hankins, B., et al. (2021). Improvements of the daily optimum interpolation sea surface temperature (DOISST) version 2.1. *Journal of Climate*, *34*(8), 2923–2939. https://doi.org/10.1175/JCLI-D-20-0166.1

Hurrell, J. W., Hack, J., Shea, D., Caron, J., & Rosinski, J. (2008). A new sea surface temperature and sea ice boundary dataset for the community atmosphere model. *Journal of Climate*, *21*(19), 5145–5153. https://doi.org/10.1175/2008JCLI2292.1

Karnauskas, K. B., Zhang, L., & Amaya, D. J. (2021). The atmospheric response to North Atlantic SST trends, 1870–2019. *Geophysical Research Letters*, *48*(2), e2020GL090677. https://doi.org/10.1029/2020GL090677

Keil, P., Mauritsen, T., Jungclaus, J., Hedemann, C., Olonscheck, D., & Ghosh, R. (2020). Multiple drivers of the North Atlantic warming hole. *Nature Climate Change*, *10*(77), 667–671. https://doi.org/10.1038/s41558-020-0819-8

Key, E. L., & Minnett, P. J. (2006). Implications of shortwave cloud forcing and feedbacks in the Southern Ocean. *Annals of Glaciology*, *44*, 15–22. https://doi.org/10.3189/172756406781811691

Kramer, S. (2025). *Modeling the global atmospheric response to persistent regional SST anomalies in the north Atlantic Ocean* (p. 31769182). University of Colorado Boulder. Retrieved from https://www.proquest.com/dissertations-theses/modeling-global-atmospheric-response-persistent/docview/3206831784/se-2

Kramer, S., & Karnauskas, K. B. (2025). ColdBlobMIP (version 1) [Dataset]. *Zenodo*. https://doi.org/10.5281/zenodo.15482718

Kramer, S. M., Karnauskas, K. B., Zhang, L., Heede, U. K., & Liu, H. (2024). A positive atmospheric feedback on the North Atlantic warming hole. *Scientific Reports*, *14*(1), 29829. https://doi.org/10.1038/s41598-024-80381-7

Li, K. Y., & Liu, W. (2025). Weakened Atlantic meridional overturning circulation causes the historical North Atlantic warming hole. *Communications Earth & Environment*, *6*(1), 416. https://doi.org/10.1038/s43247-025-02403-0

Li, L., Lozier, M. S., & Li, F. (2022). Century-long cooling trend in subpolar North Atlantic forced by atmosphere: An alternative explanation. *Climate Dynamics*, *58*(9), 2249–2267. https://doi.org/10.1007/s00382-021-06003-4

Li, X., Liu, F., Luo, Y., Zheng, X., & Wan, X. (2025). Evaluating the contribution of Asian aerosol emissions to the North Atlantic warming hole. *Journal of Climate*. https://doi.org/10.1175/JCLI-D-25-0285.1

Lindzen, R. S., & Nigam, S. (1987). On the role of sea surface temperature gradients in forcing low-level winds and convergence in the tropics. *Journal of the Atmospheric Sciences*, *44*(17), 2418–2436. https://doi.org/10.1175/1520-0469(1987)044<2418:OTROSS>2.0.CO;2

Mackay, Q., Fan, Y., Karnauskas, K. B., & Li, L. (2024). Nonstationarity of the Atlantic meridional overturning circulation's fingerprint on sea surface temperature. *Geophysical Research Letters*, *51*(19), e2024GL109789. https://doi.org/10.1029/2024GL109789

Poetzsch-Heffter, C., Liu, Q., Ruperecht, E., & Simmer, C. (1995). Effect of cloud types on the Earth radiation budget calculated with the ISCCP Cl dataset: Methodology and initial results. *Journal of Climate*, *8*(4), 829–843. https://doi.org/10.1175/1520-0442(1995)008<0829:EOCTOT>2.0.CO;2

Rahmstorf, S., Box, J. E., Feulner, G., Mann, M. E., Robinson, A., Rutherford, S., & Schaffernicht, E. J. (2015). Exceptional twentieth-century slowdown in Atlantic Ocean overturning circulation. *Nature Climate Change*, *5*(55), 475–480. https://doi.org/10.1038/nclimate2554

Rayner, N. A., Parker, D. E., Horton, E. B., Folland, C. K., Alexander, L. V., Rowell, D. P., et al. (2003). Global analyses of sea surface temperature, sea ice, and night marine air temperature since the late nineteenth century. *Journal of Geophysical Research*, *108*, 4407. https://doi.org/10.1029/2002jd002670

Richter, I., Chang, P., Chiu, P. G., Danabasoglu, G., Doi, T., Dommenget, D., et al. (2025). The tropical basin interaction model intercomparison project (TBIMIP). *Geoscientific Model Development*, *18*(9), 2587–2608. https://doi.org/10.5194/gmd-18-2587-2025

Rossby, C.-G. (1938). On the mutual adjustment of pressure and velocity distributions in certain simple current system, II. *Journal of Marine Research*, *1*(3), 239–263. https://doi.org/10.1357/002224038806440520

Smeed, D. A., McCarthy, G. D., Cunningham, S. A., Frajka-Williams, E., Rayner, D., Johns, W. E., et al. (2014). Observed decline of the Atlantic meridional overturning circulation. *Ocean Science*, *10*(1), 29–38. https://doi.org/10.5194/os-10-29-2014

Wallace, J., Mitchell, T., & Deser, C. (1989). The influence of sea-surface temperature on surface wind in the eastern equatorial Pacific: Seasonal and interannual variability. *Journal of Climate*, *2*(12), 1492–1499. https://doi.org/10.1175/1520-0442(1989)002<1492:tiosst>2.0.co;2